



Placement Matters: Understanding the Effects of Device Placement for WiFi Sensing

XUANZHI WANG, Peking University, China

KAI NIU, Peking University, China

JIE XIONG, University of Massachusetts Amherst, United States

BOCHONG QIAN, ZHIYUN YAO, and TAIRONG LOU, Peking University, China

DAQING ZHANG*, Peking University, China and Institut Polytechnique de Paris, France

WiFi-based contactless sensing has found numerous applications in the fields of smart home and health care owing to its low-cost, non-intrusive and privacy-preserving characteristics. While promising in many aspects, the limited sensing range and interference issues still exist, hindering the adoption of WiFi sensing in real world. In this paper, inspired by the SNR (signal-to-noise ratio) metric in communication theory, we propose a new metric named SSNR (sensing-signal-to-noise-ratio) to quantify the sensing capability of WiFi systems. We theoretically model the effect of transmitter-receiver distance on sensing coverage. We show that in LoS scenario, the sensing coverage area increases first from a small oval to a maximal one and then decreases. When the transmitter-receiver distance further increases, the coverage area is separated into two ovals located around the two transceivers respectively. We demonstrate that, instead of applying complex signal processing scheme or advanced hardware, by just properly placing the transmitter and receiver, the two well-known issues in WiFi sensing (i.e., small range and severe interference) can be greatly mitigated. Specifically, by properly placing the transmitter and receiver, the coverage of human walking sensing can be expanded by around 200%. By increasing the transmitter-receiver distance, a target's fine-grained respiration can still be accurately sensed with one interferer sitting just 0.5 m away.

CCS Concepts: • Human-centered computing → Ubiquitous and mobile computing systems and tools; *Ubiquitous computing; Mobile computing; Ambient intelligence.*

Additional Key Words and Phrases: Capability, WiFi Sensing, Coverage Model, Wireless Sensing, SSNR

ACM Reference Format:

Xuanzhi Wang, Kai Niu, Jie Xiong, Bochong Qian, Zhiyun Yao, Tairong Lou, and Daqing Zhang. 2022. Placement Matters: Understanding the Effects of Device Placement for WiFi Sensing. *Proc. ACM Interact. Mob. Wearable Ubiquitous Technol.* 6, 1, Article 32 (March 2022), 25 pages. <https://doi.org/10.1145/3517237>

1 INTRODUCTION

In the last decade, WiFi has become the major technology to connect computers, smartphones, electric appliances and many other IoT devices wirelessly to the Internet in indoor environment. While a huge success in data

*Corresponding author.

Authors' addresses: **Xuanzhi Wang**, Key Laboratory of High Confidence Software Technologies (Ministry of Education), school of Computer Science, Peking University, Beijing, China, xuanzhiwang@stu.pku.edu.cn; **Kai Niu**, Peking University, Beijing, China; **Jie Xiong**, University of Massachusetts Amherst, Amherst, United States; **Bochong Qian**; **Zhiyun Yao**; **Tairong Lou**, Peking University, Beijing, China; **Daqing Zhang**, School of Computer Science, Peking University, Beijing, China , Telecom SudParis and Institut Polytechnique de Paris, Evry, France, dqzhang@sei.pku.edu.cn.

Permission to make digital or hard copies of all or part of this work for personal or classroom use is granted without fee provided that copies are not made or distributed for profit or commercial advantage and that copies bear this notice and the full citation on the first page. Copyrights for components of this work owned by others than ACM must be honored. Abstracting with credit is permitted. To copy otherwise, or republish, to post on servers or to redistribute to lists, requires prior specific permission and/or a fee. Request permissions from permissions@acm.org.

© 2022 Association for Computing Machinery.

2474-9567/2022/3-ART32 \$15.00

<https://doi.org/10.1145/3517237>

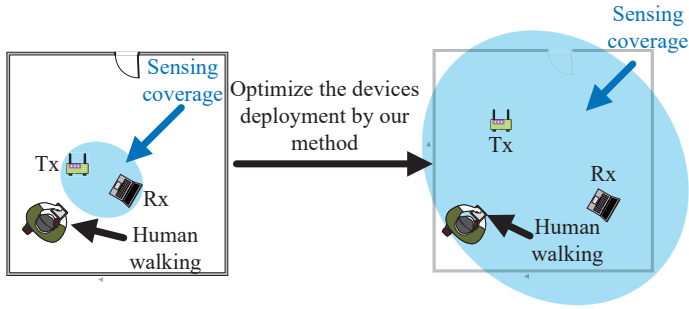


Fig. 1. The placement of transmitter and receiver can greatly affect the sensing coverage.

communication, recent effort has further exploited the pervasive WiFi signals for sensing purposes. The basic principle is that WiFi signals vary with target movements. By analyzing the signal variation, target context such as movement speed and displacement can be obtained. Promising progress has been achieved from the early attempts using WiFi CSI signals to detect human presence [8, 18, 31, 37, 49, 50], tracking human trajectory [9, 10, 17, 20, 33, 34, 36], to the latest innovations on human gesture/activity recognition [1, 4, 6, 13, 32, 41, 45, 48], vital sign monitoring [11, 14, 26, 28, 39, 46], and even material sensing [3, 43] and imaging [25]. The contact-free nature makes WiFi sensing appealing in many real-life scenarios. For example, in current Covid-19 pandemic, it is preferred a patient's respiration can be monitored in a contact-free manner. A tremendous amount of research effort has been devoted to improve the sensing accuracy [12, 14, 38, 47] and robustness [13, 47] of WiFi sensing. Despite significant progress made by the community, there are still two fundamental limits that hinder the adoption of WiFi sensing in real-world settings.

- **Small sensing range.** The first limit is the small sensing range. This is a problem not only for WiFi sensing but for all RF sensing systems due to the inherent nature of using reflection signals for sensing. Thus, there is a big gap between communication range and sensing range. While the communication range of WiFi can be tens of meters, the sensing range is merely 4-8 meters [39].
- **Strong interference.** This is because wireless sensing relies on target reflection for sensing and therefore, when there are other non-target interferers, reflections from multiple subjects get mixed at the receiver, making target sensing difficult. Because of this limit, wireless sensing is mainly restricted to single-person scenarios which may not be the case in reality.

Recent effort proposes to employ dedicated signal processing schemes [19, 39, 40] and more advanced hardware (e.g., a large antenna array [44]) to address these issues. Signal ratio scheme [39, 40] was proposed to cancel the hardware noise to increase the sensing range. Though effective, the improvement is still marginal. Researchers further propose to employ an antenna array to enable beamforming to increase the sensing range and mitigate interference by focusing the signal power at the target [44]. However, while beamforming is effective in increasing the range in communication, beamforming process corrupts the phase values which are critical for sensing. Delicate signal processing is required to recover the correct phase values to make sensing and beamforming work simultaneously [44].

In this paper, we observe an interesting phenomenon in WiFi sensing and we propose to address the above two issues from a different angle. We find that *the sensing performance of WiFi is greatly affected by the transmitter-receiver distance*. By deeply understanding the effect of transmitter-receiver distance on the sensing capability of WiFi systems, we can either increase the sensing range when there is only one single target as shown in Fig. 1 or

precisely control the sensing range to mitigate interference when there are multiple subjects. Specifically, we find that when we increase the light-of-sight (LoS) distance between the transmitter and receiver, the sensing range gets increased first and then decreased. We can therefore obtain the maximum coverage by properly placing the transmitter and receiver. It is more interesting to see that a very small sensing range can be achieved when the transmitter-receiver distance is more than 10 meters and we can leverage this small sensing coverage which is traditionally considered as a disadvantage to mitigate the severe interference issue in WiFi sensing. By planning the placement of the transmitter and receiver, we can restrict the sensing only within a targeted boundary. We believe this is an important step toward real-world adoption of wireless sensing.

We also show people that to quantify the sensing capability, the widely used signal-to-noise-ratio (SNR) metric in communication is not appropriate and we propose a new metric which can capture the unique characteristics of RF sensing to help people understand the sensing performance and guide the sensing system design accordingly. Through both theoretical analysis and experiment, we validate the effectiveness of the proposed metric in quantifying the sensing capability.

To summarize, the main contributions of this work are as follows.

- Inspired by the SNR metric in communication, we propose a metric named SSNR (sensing-signal-to-noise-ratio) to quantitatively characterize the sensing capability of CSI signals in WiFi sensing systems. This metric can be generalized to quantify the sensing capability of other sensing modalities such as acoustic sensing and UWB sensing.
- Based on the new metric, we model the relationship between the sensing coverage and the transmitter-receiver distance, unmasking the effect of transmitter-receiver distance on sensing coverage. Comprehensive real-world experiments are conducted to validate the correctness of the theoretical model.
- With the proposed quantitative model, we find that the sensing coverage area does not always monotonically increase with an increasing transmitter-receiver distance. Specifically, in LoS scenario,¹ the sensing coverage increases first from a small oval to a maximal one and then decreases to a peanut shape. The peanut shape is separated into two ovals located around the two transceivers respectively when the transmitter-receiver distance further increases.
- Guided by the interesting observations, two critical challenges in WiFi sensing can be addressed: (a) the limited WiFi sensing area can be increased and (b) the severe interference in real-world settings can be mitigated by controlling the transmitter-receiver distance. Two representative application scenarios are employed to demonstrate the effectiveness of the proposed model. In a single-person scenario, the sensing coverage of human walking detection can be extended by around 200% compared with the commonly adopted deployment strategies. In a multi-person scenario, the fine-grained human respiration can be accurately monitored without being interfered by a close-by person.

2 RELATED WORK

In this section, we briefly review the related work on RF-based contactless sensing systems and group them into two categories: radar-based and WiFi-based approaches.

2.1 The Sensing Coverage of Radar Systems

In radar systems, the sensing coverage has been explored in depth [2, 7, 16, 21–23]. For radar systems, as the noise power in an outdoor environment is regarded roughly a constant, the sensing coverage of a radar system mainly relies on the received signal power reflected from the target. In order to make a target detectable by a radar system, the reflected signal has to be larger than a threshold. To enlarge the sensing range, radar systems either employ directional antenna to increase the signal power of reflections, or reduce the noise power by adopting

¹The more complicated non-LoS scenario can be modeled by taking the attenuation of the occlusions into consideration.

advanced electronic components and signal filters. Note that the static power through LoS is not considered in radar systems as directional antennas are usually adopted.

2.2 The Sensing Coverage of WiFi-Based Sensing Systems

Compared to radar systems, very little attention has been dedicated to the sensing coverage issue in WiFi sensing. In 2011, Neal et al. [15] presented a statistical model to characterize the RSS (Received Signal Strength) variance as a function of a target's position with respect to the transmitter and receiver locations for localization. In 2012, Wu et al. [35] leveraged the channel state information (CSI) to build a device-free localization system FILA, which proved to achieve higher accuracy than RSS-based solutions. They developed a refined indoor propagation model to represent the relationship between the CSI and distance by revising the free space path loss propagation model to estimate a target's location with CSI.

In 2018, Xin et al. [37] proposed FreeSense, a WiFi-based human detection system. In order to estimate the sensing range for human detection, they only considered the reflection signals from a target and adopted the Fresnel Zone theories [42] to model the sensing boundary as ellipses, and further concluded that the size of coverage will increase as the distance between transmitter and receiver increases. This conclusion is correct when the LoS path length is relatively small. We demonstrate in this work that the sensing coverage actually decreases when the LoS path is further increased.

Different from the above-mentioned work, we propose a new metric to quantify the sensing capability of WiFi sensing systems and study the sensing coverage both theoretically and experimentally. We discover several properties which can be leveraged to guide WiFi sensing system deployment and we believe the findings can be applied to benefit other sensing modalities such as acoustic, LoRa and UWB sensing.

3 PRELIMINARY

In this section, we introduce the background knowledge of WiFi sensing. In a typical WiFi sensing system as shown in Fig. 2, besides the LoS direct path signal between the transmitter and receiver, the WiFi signals also get bounced off objects in the environment such as the sofa and the human body. These signal propagation paths can be divided into two categories: *static path* and *dynamic path*. The static paths (green lines in Fig. 2) include the LoS path and the reflection paths from static objects in the environment. The target movement, on the other hand, induces dynamic signal paths (yellow line in Fig. 2). At the WiFi receiver, channel state information (CSI) is leveraged to characterize the signal propagation through multiple paths. Given a WiFi channel with a central frequency f , the CSI ($H(f, t)$) of this channel at time t can be expressed as $H(f, t) = Y(f, t)/X(f, t)$, where $X(f, t)$ and $Y(f, t)$ are the frequency domain representations of the transmitted and received signals, respectively [27]. The CSI can be represented as a linear superposition of all the paths including the dynamic path ($H_d(f, t)$), static path ($H_s(f, t)$) and noise ($H_n(f, t)$):

$$\begin{aligned} H(f, t) &= H_s(f, t) + H_d(f, t) + H_n(f, t) \\ &= |H_s(f, t)|e^{-j\theta_s} + |H_d(f, t)|e^{-j \cdot 2\pi \frac{d(t)}{\lambda}} + |H_n(f, t)|e^{-j\theta_n}. \end{aligned} \quad (1)$$

$|H_s(f, t)|$, $|H_d(f, t)|$, and $|H_n(f, t)|$ are the amplitude of each CSI component. θ_s and θ_n represent the phases of the static path signal and noise, respectively. $e^{-j \cdot 2\pi \frac{d(t)}{\lambda}}$ represents the phase of the dynamic path with a changing path length of $d(t)$. The three signal components (H_d , H_s and H_n) are also illustrated in the I-Q space in Fig. 3. Fig. 4 plots the CSI samples received at a WiFi receiver. The green line represents the static signal, which can be calculated by averaging the CSI samples over a period of time (e.g., one cycle of respiration). The noise renders the collected signal (blue line) deviate from the ideal signal (orange line). We extract the variation of the composite signal to infer the target's movement.

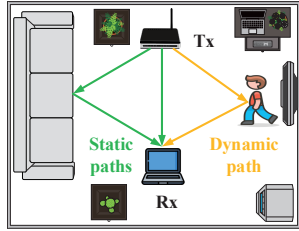


Fig. 2. WiFi signal propagation can be grouped into two categories: static path signal and dynamic path signal.

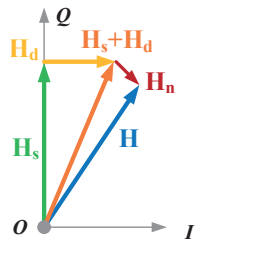


Fig. 3. The vector representation of CSI components in the I-Q space.

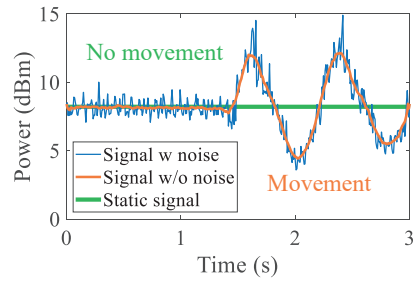


Fig. 4. The power components of CSI samples.

4 QUANTIFYING THE SENSING CAPABILITY OF WIFI SYSTEMS

In this section, we first introduce the widely-used SNR (signal-to-noise-ratio) metric for communication. Then we propose the new metric to quantify the WiFi sensing capability.

4.1 The SNR Metric for WiFi Communication

In WiFi communication systems, SNR is used to quantify the communication capability of the received signal. If the SNR is lower than a threshold, communication may fail due to a high bit error rate. Specifically, SNR can be expressed as [24]:

$$SNR = \frac{P_r}{P_n} = \frac{|H_s(f, t) + H_d(f, t)|^2}{|H_n(f, t)|^2}, \quad (2)$$

where P_r is the power of the received signal and P_n is the power of noise. $H_s(f, t)$ and $H_d(f, t)$ are the signals arriving through static path and dynamic path, respectively. Note that both static path signal and dynamic path signal can be used for communication. The denominator is additive white Gaussian noise.

4.2 The New SSNR Metric for WiFi Sensing

Different from communication, in WiFi sensing, only the dynamic signals reflected from the target contain the sensing information. Static signals such as the LoS signal and reflections from walls do not contain target information and therefore can not contribute to sensing. Therefore, it is not appropriate to use the SNR designed for communication to characterize the sensing capability. What is interesting is that in WiFi sensing, in addition to thermal noise which influences the extraction of the dynamic signal for sensing, the static signal also has a negative effect on sensing. In this work, we propose a new metric SSNR (sensing-signal-to-noise-ratio) to quantify

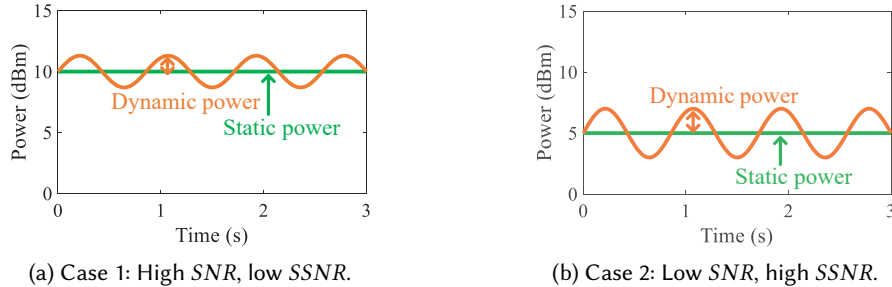


Fig. 5. The communication metric SNR versus the sensing metric $SSNR$.

the sensing capability as below:

$$SSNR = \frac{P_d}{P_i} = \frac{|H_d(f, t)|^2}{|g(H_s(f, t)) + H_n(f, t) + H_i(f, t)|^2}, \quad (3)$$

where P_d is the power of the dynamic signal reflected from target, and P_i contains the thermal noise ($H_n(f, t)$),² the effect of other dynamic subjects, i.e., interferers ($H_i(f, t)$), and also interference ($g(H_s(f, t))$) induced by the static signal ($H_s(f, t)$). When there are interferers, SSNR is decreased. When the interferers are close to the target, the SSNR value can be significantly reduced, degrading the sensing performance. When there is only one target without any interferers, the metric SSNR in Equation 3 can be simplified as below:

$$SSNR = \frac{P_d}{P_i} = \frac{|H_d(f, t)|^2}{|q(H_s(f, t)) + H_n(f, t)|^2}. \quad (4)$$

Compared with interference, thermal noise is much smaller. To study the effect of interference induced by the static signal, we conduct experiments in Section 4.3. From Equation 4, we can see that the numerator contains only the power of the dynamic signal reflected from the target and the denominator contains both thermal noise and interference induced by static signal, which is different from that in communication.

As illustrated in Fig. 5, we present two cases to compare the communication metric SNR and sensing metric SSNR in WiFi systems. As the power of the signal in Case 1 (Fig. 5a) is larger than that in Case 2 (Fig. 5b), the corresponding SNR and communication capability of Case 1 is higher than that in Case 2. However, the variation of the signal corresponding to the dynamic signal power in Case 2 is larger than that in Case 1, presenting a higher SSNR and accordingly a higher sensing capability. This example demonstrates that the newly defined metric SSNR can better characterize the sensing capability in WiFi systems.

4.3 Characterizing Interference Caused by Static Signal

In our empirical studies, we notice that besides the thermal noise, the static power also causes interference and affects the sensing performance. To investigate the effect of static signal on sensing, we conduct benchmark experiments to characterize the effect.

4.3.1 Experiment setup. We employ both software-defined radio platform (WARP V3) and commodity hardware (Intel 5300 NIC card) to conduct benchmark experiments as shown in Fig. 6.

²Under the experiment conditions in this paper, the temperature has a relatively small effect on thermal noise. Specifically, for 20 MHz bandwidth WiFi signal, the thermal noise only increases from -101.073 dBm to -100.77 dBm when temperature changes from 10 °C to 20 °C.



Fig. 6. Setup of benchmark experiments.

- *WARP V3 platform:* One WARP platform is employed with two RF ports serving as the transmitter and receiver, respectively. Both the transmitter and receiver are equipped with one omni-directional antenna. The transmitter sends out WiFi packets at 1500 pkt/s on the 5.32 GHz WiFi band with a channel bandwidth of 20 MHz.
- *Intel 5300 WiFi card:* We leverage the open-sourced CSITool [5] to collect CSI samples from Intel 5300 card. One MiniPC equipped with one Intel 5300 WiFi card is configured as the transmitter while another MiniPC with 5300 card serves as the receiver. The transceivers are equipped with the same omni-directional antennas. The central frequency and bandwidth of WiFi signals are set to 5.64 GHz and 20 MHz, respectively.

The antennas on both the transmitter and receiver are placed roughly at the same height as the target. We vary the static power to examine the relationship between the interference and static power.

Experiment 1: Different LoS path lengths. To verify the relationship between static power and interference power under different LoS settings, we vary the length of the LoS path from 1 m to 7 m at a step size of 1 m in a meeting room as shown in Fig. 7a. For each setting, we calculate the static power as the average of the collected CSI amplitudes³ within a small window of 0.1 s, while the interference power⁴ is calculated as the difference between the raw CSI amplitude and the averaged CSI amplitude.

Experiment 2: Different environments. We conduct experiments in three different indoor environments including a meeting room ($7.8 \text{ m} \times 8.4 \text{ m}$), an office room ($6.8 \text{ m} \times 7.8 \text{ m}$) and a corridor ($1.95 \text{ m} \times 8.4 \text{ m}$), as shown in Fig. 7. In this experiment, the distance between the transceivers is fixed as 2 m. We move the transceiver pair to different positions in each environment to vary the static signal propagation path to obtain different static powers. We would like to verify the relationship between the static power and interference power is environment-independent.

Experiment 3: Different obstacle locations blocking the LoS path. We employ a metal plate with a size of $35 \text{ cm} \times 40 \text{ cm}$ to study the effect of the obstacle in the meeting room. In particular, we place the metal plate at different locations between the transmitter and receiver to vary the static power. The metal plate is placed between the transceivers as shown in Fig. 6 and we vary the static power by moving the metal plate. As shown in Fig. 8a, when the LoS path length is 1 m, the metal iron plate is placed at the two ends and also the middle point of the transceivers respectively. When the LoS path length is 2 m-7 m, the metal plate is placed at different positions at a step size of 1 m as shown in Fig. 8b. We then collect the CSI samples and calculate the interference power and static power accordingly.

³Note that the CSI amplitude retrieved from Intel 5300 WiFi cards actually represents the signal power.

⁴The interference power measured also contains the thermal noise. The thermal noise part is much smaller than the interference caused by the static signals.

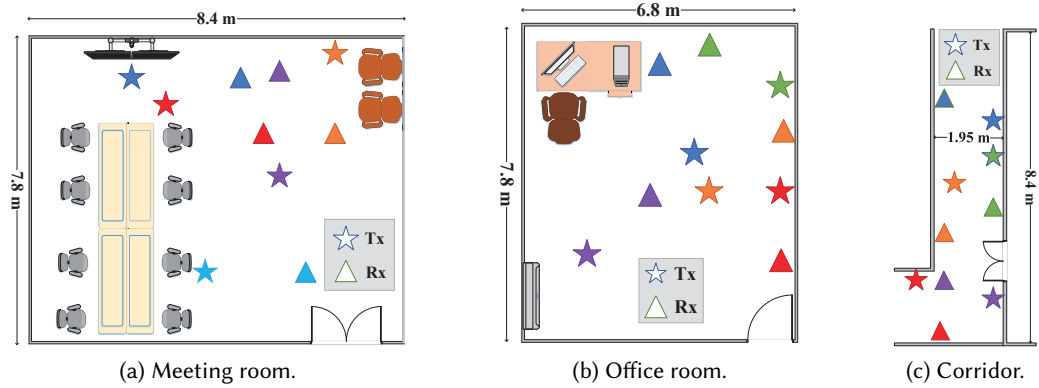


Fig. 7. Experiment setup in three indoor environments.

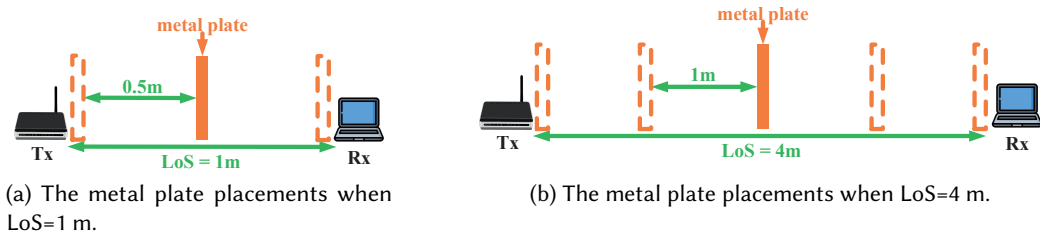


Fig. 8. Verify the effect of obstacle blocking by placing the metal plate at different locations.

4.3.2 Results analysis. Fig. 9 shows the experiment results with the WARP platform. The x-axis represents the estimated static power and the y-axis indicates the interference power. The blue line is the fitted curve using a linear fitting with the least square method. We observe that the interference power is in proportion to the static power across all three experiments. The slopes estimated in three environments are 0.0127, 0.0121, and 0.0127 respectively. We can see that the slopes are roughly the same. Fig. 10 illustrates the experiment results with commodity WiFi devices. Though the variance of interference power is larger than that of WARP platform, the linear relationship between interference power and static power still holds. The slopes in the three environments are 0.0247, 0.0250, and 0.0240, respectively. From our experiments, we conclude that the slope is hardware dependent and environment independent. In summary, these experiments demonstrate that interference power is linearly related to the static power.

5 MODELING THE SENSING COVERAGE IN WIFI SYSTEMS

In this section, we first present the analytical relationship between sensing coverage and the LoS distance of transceivers in *free space*, and then extend it to the *multipath* prevalent indoor scenario. Finally, we summarize the key properties extracted from the relationship analysis to guide our system design.

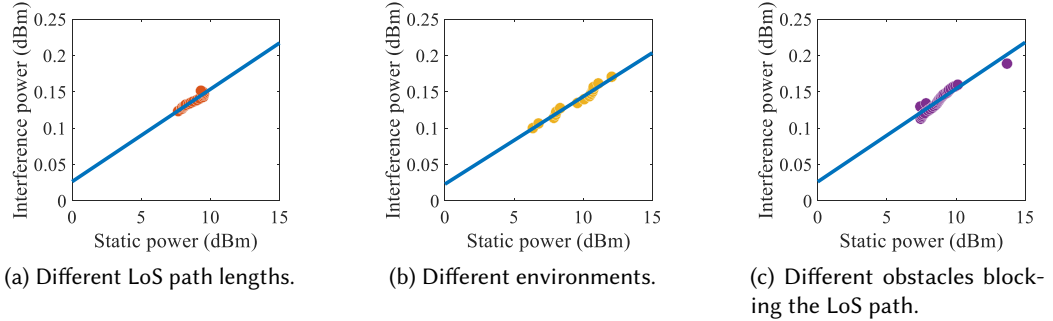


Fig. 9. The experiment results using WARP platform.

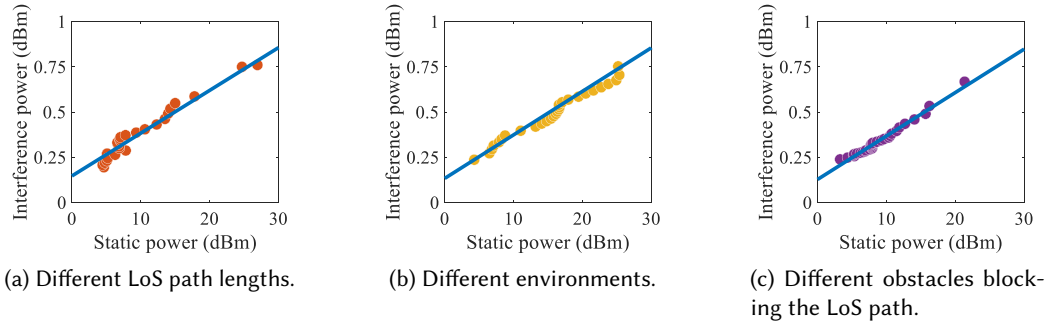


Fig. 10. The experiment results using commodity WiFi devices.

5.1 The Sensing Coverage Model in Free Space

We start with establishing the sensing coverage model in free space where no static reflection paths exist. According to [29], the power of the dynamic signal can be expressed as:

$$P_d = \frac{P_t G_t G_r \lambda^2 \sigma}{(4\pi)^3 (r_T r_R)^2}, \quad (5)$$

where P_t is the transmission power. G_t and G_r are the antenna gains at the transmitter and receiver, respectively. λ is the signal wavelength and σ is the effective reflection area of the target. r_T and r_R are the distance from the target to the transmitter and receiver, respectively. In free space, the static path is the LoS path and the signal power can be denoted as:

$$P_{LoS} = \frac{P_t G_t G_r \lambda^2}{(4\pi)^2 r_D^2}, \quad (6)$$

where r_D is the path length of LoS. As the interference power P_i is linearly proportional to the static power, the interference power can be further expressed as:

$$P_i = \gamma P_{LoS} + b = \gamma \frac{K}{r_D^2} + b, \quad (7)$$

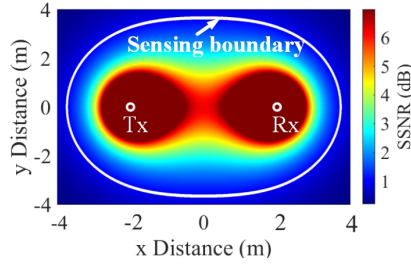


Fig. 11. The heatmap of sensing capability for a given transceiver pair. The red color means strong sensing capability, while the blue color indicates weak sensing capability.

where γ is the slope of the linear curve, b is a constant and $K = \frac{P_t G_t G_r \lambda^2}{(4\pi)^2}$. From extensive experiments, we observe that γ and b have fixed values for a given WiFi device. Since the thermal noise P_n can be assumed as a constant within a short period of time, we just use b to represent all the constant parts of the noise. The SSNR metric proposed to quantify the sensing capability can be presented as:

$$\text{SSNR} = \frac{P_d}{P_i} = \frac{\frac{K\sigma}{4\pi(r_T r_R)^2}}{\gamma \frac{K}{r_D^2} + b} = \frac{K\sigma}{4\pi(r_T r_R)^2(\gamma \frac{K}{r_D^2} + b)}. \quad (8)$$

Given a WiFi transmitter-receiver pair, the transmission power P_t , antenna gains G_t and G_r , and signal wavelength λ can be viewed as constants. γ and b are also constants and can be measured in advance. If we assume the target reflection area is a constant and b is small, Equation 8 can be simplified as:

$$\text{SSNR} \propto \frac{r_D^2}{(r_T r_R)^2}, \quad (9)$$

where r_T and r_R are the distances from the target to the transmitter and receiver, respectively. r_D is the distance between the transmitter and receiver. From Equation 9, we observe that the sensing capability of a WiFi system is related to the distance between transceivers (r_D) and the target's distance to the transceivers (r_T and r_R). We first investigate how the sensing capability varies with the target's location for a fixed LoS length (r_D). Fig. 11 presents the heatmap of sensing capability for a transmitter-receiver pair. We can see the SSNR value keeps a constant at locations with the same $r_T \cdot r_R$ value. These locations indeed form a Cassini oval where the product of its distances to the transmitter and receiver is a constant. Besides, the size of Cassini oval shrinks with the increase of SSNR and finally collapses into two separate ovals around the transmitter and receiver, respectively. This observation is validated with experiments in Section 6.1.

We can now theoretically know the sensing capability of each location. The minimum SSNR requirement differs with sensing applications. Based on the minimum SSNR requirement, the sensing boundary can be represented as:

$$(r_T r_R)_b \propto \sqrt{\frac{r_D^2}{\text{SSNR}_{min}}}. \quad (10)$$

We next investigate the effect of LoS path length on sensing boundary. Fig. 12 illustrates the sensing boundary of WiFi sensing system with different LoS path lengths. Fig. 13 shows the size of the sensing coverage area under different LoS path lengths. Note that only half the plane is considered when we calculate the size of the sensing area in this work. It is interesting to see that the sensing area increases first and then decreases with the

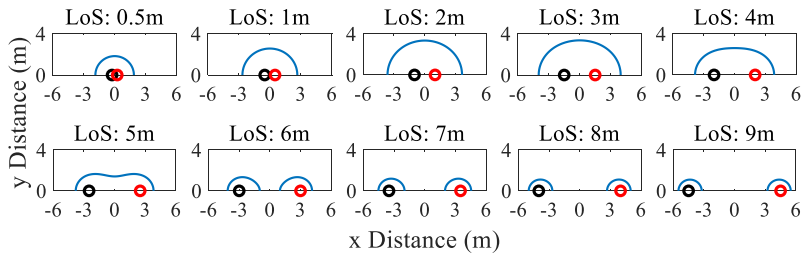


Fig. 12. The sensing coverage boundary under different LoS path lengths.

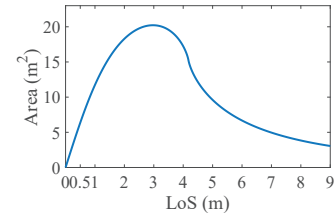


Fig. 13. The size of the sensing area under different LoS path lengths in free space.

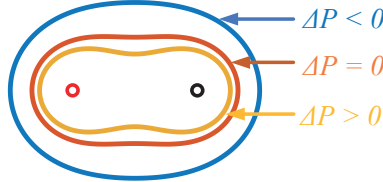


Fig. 14. The sensing coverage boundary in the multipath-rich environment: the sensing coverage can be either increased (blue line) or decreased (yellow line).

increasing of LoS path length, which indicates the sensing coverage can be manipulated by tuning the deployment of transceivers. In reality, there are always multipath reflections from surroundings. We next discuss how the sensing boundary looks like with multipath in the indoor environment.

5.2 Extending the Sensing Coverage Model to Work in Multipath-Rich Environment

Unlike the free space where the transmission signal only bounces off the targeting object, the transmission signal bounces off walls, chairs, and many other objects in a real indoor environment. Therefore, the static power is no longer equal to the power of the LoS path. Instead, the static power is determined by the superposition of all static paths. To extend the sensing coverage model to the multipath rich environment, we use ΔP to represent the power change induced by multipaths and Equation 10 can be rewritten as:

$$(r_T r_R)_b = \sqrt{\frac{K}{4\pi(\gamma(P_{LoS} + \Delta P) + b)SSNR_{min}}}. \quad (11)$$

When the multipath signals constructively combine with the LoS signal, $\Delta P < 0$. Based on Equation 11, the denominator decreases, and the sensing boundary increases.

As shown in Fig. 14, the red line is the original sensing coverage without multipaths. The blue line indicates that the multipaths enlarge the sensing boundary ($\Delta P < 0$), while the yellow line shows that the multipaths reduce the sensing boundary ($\Delta P > 0$). These results demonstrate the feasibility of tuning the sensing area coverage through static power control. Besides varying the LoS path length, we can also change the multipath to vary the sensing boundary.

5.3 Key Properties of the Sensing Coverage Model

With the above theoretical analysis, we summarize the key properties of the WiFi sensing coverage with respect to the LoS length.

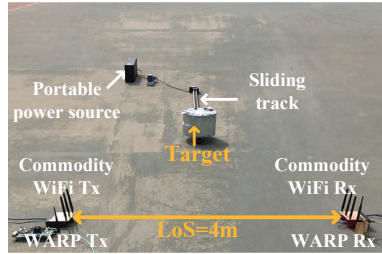


Fig. 15. Experiment setup to verify the proposed sensing coverage model.

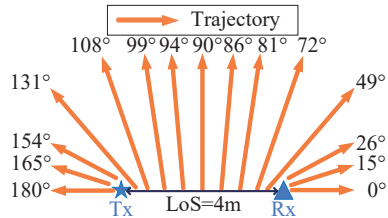


Fig. 16. The 15 track trajectories to move the metal cylinder.

- 1) The sensing capability isoline in WiFi sensing takes the shape of Cassini ovals with the two foci at the locations of the transceivers.
- 2) When the LoS path length is short (0.2 m - 1 m), the sensing coverage is a small oval. Due to the small sensing coverage, the device can only sense human activities at a short distance. We can leverage this property to design a co-located transmitter-receiver pair and place them close to the target to mitigate the interference issue in sensing.
- 3) When the LoS path length is moderate (1 m - 6 m), the sensing coverage is an oval, and the sensing coverage is large. The sensing coverage can be further expanded by reducing the static power through multipath control.
- 4) When the LoS path length is relatively large (larger than 6 m), the sensing coverage is two small circles surrounding the two transceivers as shown in Fig. 12. In this case, it only has the capability to sense the regions near to the transceivers. This property can also be leveraged to sense only a targeted region and mitigate the well-known interference issue in WiFi sensing.

6 EVALUATION

In this section, we first conduct benchmark experiments to validate the key properties of WiFi sensing systems. Then we leverage the properties obtained in this work to guide the system design of human walking detection and respiration monitoring under various conditions.

6.1 Verify the Key Properties of Sensing Coverage Model

Experiment setup. The experiment setup is identical to that in Section 4. Note that although Intel 5300 card has three antennas connected, only one is used in our experiment. For all the collected data samples, we first apply a Hampel filter to denoise the raw CSI amplitude signal using a sliding window of 0.15 s with overlapping of 0.1 s. Then the static signal power can be calculated as the average CSI amplitude within the observation window. The maximum value of the difference between the CSI amplitude and the averaged amplitude within the observation window indicates the dynamic power. The interference power is calculated as the difference before and after filtering the CSI amplitude.

- 1) **Experiment 1:** Verify the spatial distribution of sensing capability. We first conduct an experiment to verify the spatial distribution of sensing capability using both WARP software-defined radio platform and commodity WiFi hardware. In the experiments, we employ a sliding track to move a metal cylinder which is an ideal reflector (Fig. 15). The sliding track can be precisely controlled at an accuracy of 0.5 mm. As shown in Fig. 16, the length of the LoS path is set as 4 m and 15 trajectories are chosen to move the cylinder. For each trajectory, the sliding track is employed to move the metal cylinder in the directions indicated by the orange arrow. Note that as the cylinder moves further, signal fluctuations [26, 34] and accordingly SSNR become smaller,

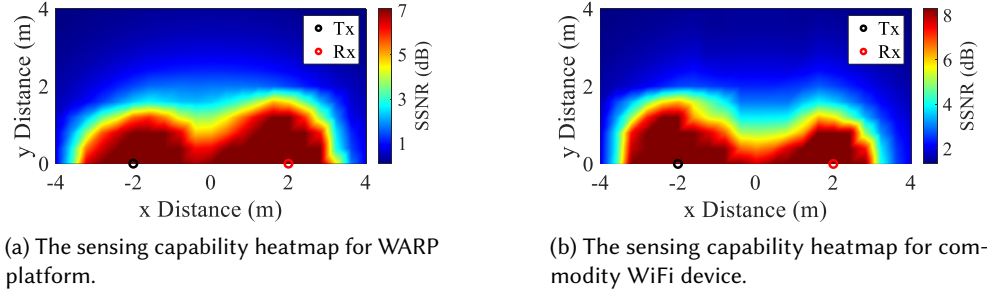


Fig. 17. The sensing capability distribution.

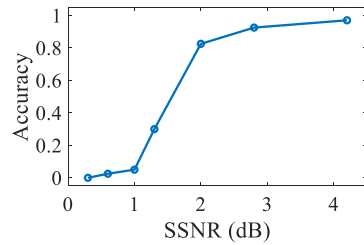


Fig. 18. SSNR v.s. speed estimation accuracy.

and eventually the cylinder movement cannot be detected. Fig. 17 shows the heatmaps of sensing capability for both WARP platform and commodity WiFi device. Red color means a good sensing capability while blue color indicates a poor sensing capability. The Cassini ovals can be clearly observed, matching the theoretical analysis in Section 5.1 very well.

- 2) **Experiment 2:** Verify the effectiveness of using the proposed SSNR metric to determine the sensing boundary. In this experiment, we track the metal cylinder's moving at different directions as shown in Fig. 16. The speed estimation accuracy and the average SSNR of the received signals at seven positions are shown in Fig. 18. We can see that the speed estimation accuracy increases as SSNR increases. When SSNR value exceeds 2 dB, the accuracy is greatly improved and gradually saturates.

To obtain the performance-based sensing (SP) boundary, we consider the target's moving is not detectable when the speed estimation accuracy is below 80%. For the SSNR-based scheme, we choose SSNR=2 dB to determine the sensing boundary. Fig. 19 shows the boundaries obtained by the two methods, which are very close to each other for both WARP and commodity WiFi platforms. These results validate the effectiveness of our proposed SSNR metric to determine the sensing boundary.

- 3) **Experiment 3:** Verify the effect of LoS path length on sensing coverage. In this experiment, we verify the effect of LoS length on the sensing coverage revealed in Section 5.1. The experiment setup is identical to Experiment 1. The LoS length is varied from 1 m to 7 m at a step size of 1 m. Fig. 20 shows the sensing area obtained with WARP platform and commodity WiFi devices (orange line) and corresponding simulation results (blue line). We can observe that the experiment results match the simulation curves very well except small LoSs (i.e., 0.5 and 1 m). The reason behind is that the target reflection area in experiments is slightly smaller than that in simulation. Specifically, the sensing area grows first and then drops for both platforms.

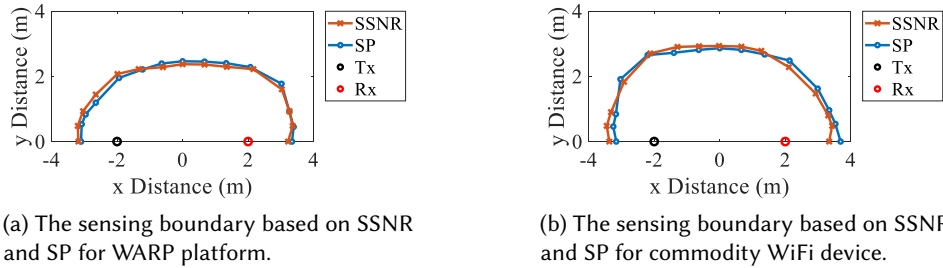


Fig. 19. Verify the effectiveness of our proposed SSNR metric to determine the sensing boundary.

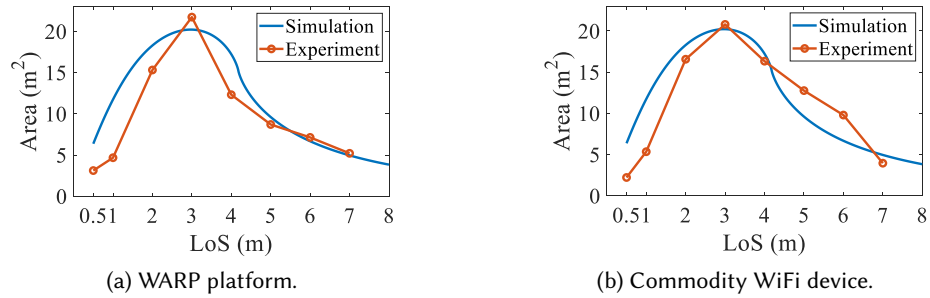


Fig. 20. Verify the effect of LoS length on the sensing coverage.

- 4) **Experiment 4:** Verify the effect of multipath on the sensing coverage. We also conduct benchmark experiments in an indoor environment (Fig. 7b) to evaluate the effect of multipaths. The experiment setup is the same as that in Experiment 1. We vary the static power by fine-tuning the transceivers' locations to change the multipaths. Note that we make sure the LoS distance between the transmitter and receiver is the same during the tuning process. Fig. 21 shows that decreasing the static power enlarges the sensing coverage. These results demonstrate that when the transmitter-receiver distance is constant, the size of the sensing coverage can still be tuned by controlling the static power through multipath. In this experiment, we control the static power by moving the transmitter-receiver at the same time. The static power can also be controlled by moving the objects indoors and even injecting virtual multipath in software [14] without a need to physically move the transceivers. Note that the SNR for communication is not affected much during the process of tuning the SSNR due to the small LoS path length in indoor settings.
- 5) **Experiment 5:** Verify the effect of temperature and humidity on the sensing boundary. We conduct a group of experiments to verify the influence of temperature and humidity on the sensing boundary. For a small propagation distance (e.g., a few meters), humidity and temperature have little influence on the propagation of electromagnetic waves with a frequency below 10 GHz [51]. The length of the LoS path is set as 3 m and the other setting is consistent with that in Experiment 1. To evaluate the effect of temperature, we fixed the relative humidity as 35%, and increased the temperature from 10 °C to 25 °C with the help of an air conditioner. To evaluate the effect of humidity, we fixed the temperature as 10 °C, and increased the relative humidity from 35% and 55% using a humidifier. Note that most indoor environments have a relative humidity between 35% to 60% [30]. The results are shown in Fig. 22a and we can see that the sensing boundaries are roughly the same

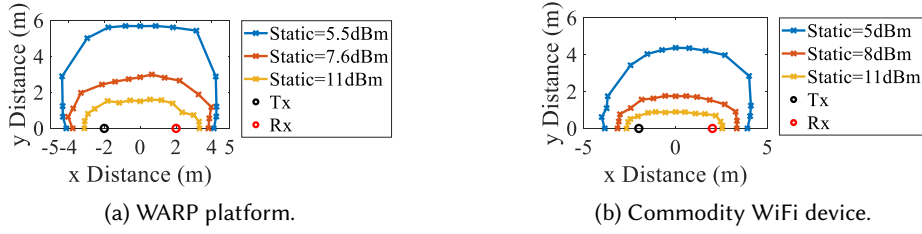


Fig. 21. Verify the effect of multipath on the sensing coverage.

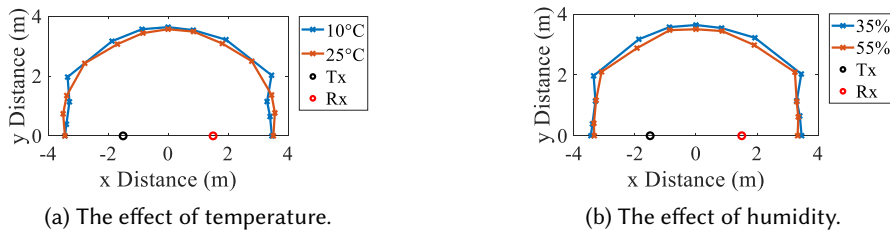


Fig. 22. Verify the effect of temperature and humidity on the sensing boundary.

when the temperature differs by 15 °C. Fig. 22b shows that the sensing coverage shrinks only slightly when the humidity is increased by 20%. We believe if 60 GHz mmWave signals are used for sensing, the sensing boundary can be affected more by humidity. We can then even use the sensing range change to estimate the humidity information in a room.

6.2 Boosting the Sensing Coverage of Human Walking Detection

The sensing range of WiFi is quite limited if the device placements are not properly planned. In a typical bedroom environment with a size of 4.5 m × 5.5 m, we observed that only around 40% of the area can be covered if we randomly mounted the WiFi receiver at one corner of the room and placed the transmitter on the bedside table. We show that by applying the theories developed in this work to guide our transceiver placement, we can significantly increase the sensing coverage to cover the whole room as shown in Fig. 23. From our analysis in Section 5, we can tune the LoS distance between the transceivers to boost the sensing coverage.

Two Mini-PCs equipped with Intel 5300 COTS WiFi cards are employed as transceivers to conduct experiments. The transceivers are placed at a height of 1.1 m from the ground using tripods. The room has a size of 4.5 m × 5.5 m. Through our theoretical analysis, the transmitter and receiver need to be placed with a distance of 3 m to achieve the largest sensing coverage. We further measure the static power of multiple 3 m transmitter-receiver placements to identify the one with the minimum static power which theoretically presents us the largest sensing coverage. To see the effect of this deployment, we compare the sensing coverage under three different deployment strategies: S1) Randomly placing the transmitter and receiver at a distance of 2 m; S2) Randomly placing the transmitter and receiver at a distance of 3 m; and S3) Placing the transmitter and receiver at a distance of 3 m and further choosing the deployment with the smallest static power. To evaluate the sensing coverage performance, we pick 153 (17 × 9) locations evenly distributed in the room and test at how many locations the human walking can be detected under the three deployment strategies. Our results show that under deployment strategy 1, we can

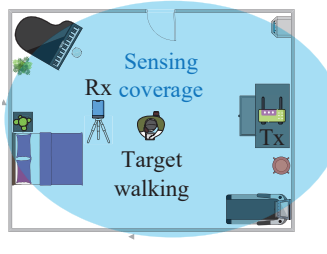


Fig. 23. Increase the sensing coverage to cover the whole room.

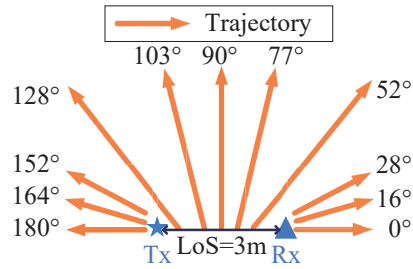


Fig. 24. The human walking trajectories.

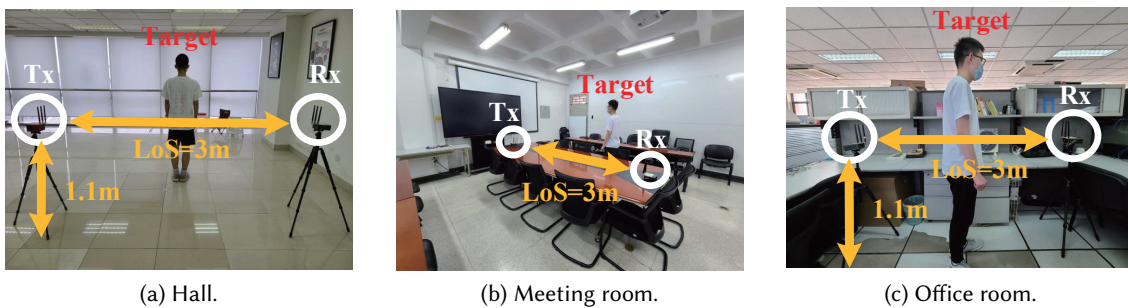


Fig. 25. Experiment setup in three environments.

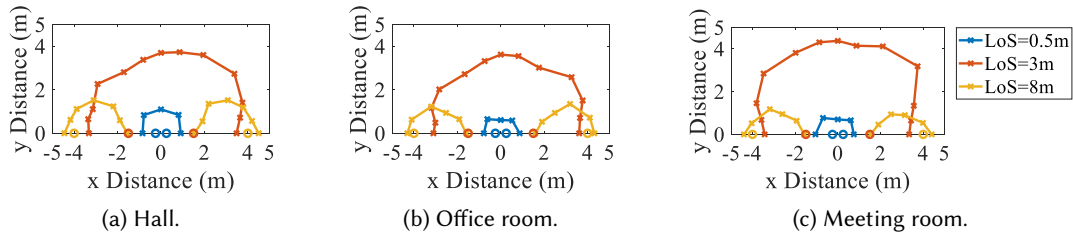


Fig. 26. Impact of environment on the sensing area of human walking.

detect human walking at 68 out of the 153 locations. This number increases to 102 and 124 under deployment strategy 2 and strategy 3, respectively. These results clearly demonstrate the correctness of the proposed theory and the effectiveness of applying it to guide our deployment in increasing the sensing coverage.

Next, we evaluate the impact of environments, user diversity, furniture layout and Tx-Rx height difference on sensing coverage.

- **Impact of environment.** We conduct experiment in three typical environments with different amounts of multipath, i.e., a large hall with little multipath (Fig. 25a), a meeting room with medium amount of multipath (Fig. 25b), and a graduate student office with rich multipath (Fig. 25c). The LoS path length between the transmitter and receiver is set as 0.5 m, 3 m, and 8 m. Fig. 26 shows the sensing coverage is maximum (orange line) when the LoS path length is 3 m for all environments. When LoS path length is

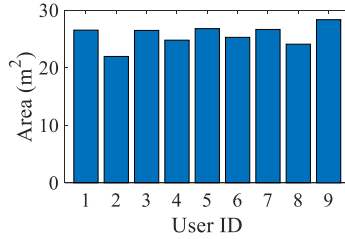


Fig. 27. Impact of user diversity on the sensing area of human walking detection.

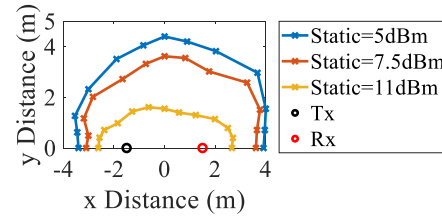


Fig. 28. Impact of furniture layout on boosting the sensing area of human walking detection.

0.5 m, the sensing coverage is a small circle (blue line). For comparison, when LoS is 8 m, the coverage area is separated as two small circles (yellow line). The experiment results match the theoretical plots well. Note that the sensing range can be increased or decreased with multipath. If the multipath destructively combines with the LoS path, the sensing range is increased and vice versa.

- **Impact of user diversity.** In this experiment, we recruit 9 participants including 3 females and 6 males to verify the impact of user diversity under a LoS length of 3 m. The height of the participants varies from 160 cm to 180 cm and the weight ranges from 45 kg to 100 kg. As illustrated in Fig. 27, the sensing areas for all the participants are above $22 m^2$ under a LoS length of 3 m. We do observe some differences among users. We believe this is because the size of the reflection area varies with the user's body size. Among the 9 participants, participant 9 has the maximum weight and size and accordingly a maximum sensing area of $28.36 m^2$ is achieved.
- **Impact of furniture layout.** Next, we consider the meeting room environment (Fig. 25b) in which furniture (e.g., tables, chairs, etc.) is added to the environment. The static reflection paths get changed and we move the furniture location to fine-tune the static power to 5 dBm, 7.5 dBm and 11 dBm respectively. As shown in Fig. 28, the sensing coverage area varies dramatically. When the static power is 11 dBm, the sensing area is decreased to $6.5 m^2$ and when the static power is 5 dBm, the sensing area is $26.2 m^2$. This demonstrates the feasibility of controlling the sensing coverage through static power tuning. The results also match the theories well in Section 5.2. However, we also note that it is very difficult to tune the static power to very small. This is because the power via LoS path is stronger than that via the reflection path, and therefore it is difficult to totally cancel it out. Also, the interference power always exists.
- **The effect of Tx-Rx height difference.** In real-world settings, the transmitter and receiver may not be at the same height. We now study the effect of height difference between transceivers on the proposed sensing coverage model. As shown in Fig. 29, the horizontal distance between the transmitter and receiver is set to 2 m and 3 m, respectively. We increase the height difference between the transceivers from 0 m to 2 m at a step size of 1 m. The experiment setting is the same as that in Section 6.2, and the height of the transmitter is adjusted using a tripod as shown in Fig. 30.

The results are shown in Fig. 31a and Fig. 31b. In Case 1, the transceivers are at the same height. The sensing boundaries are represented by the blue line in Fig. 31a and Fig. 31b. Case 2 represents the case when the height difference between the transmitter and receiver is 1 m. We can observe that the sensing boundaries (red lines) are similar to Case 1 (blue lines). In Case 3, the height difference between the transmitter and receiver is increased to 2 m. The sensing boundaries (yellow lines) are slightly smaller near the transmitter. The boundaries near the receiver are still roughly the same. To conclude, when the height difference is small, the effect on sensing coverage is limited. When the height difference is increased to

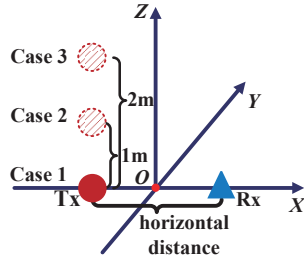


Fig. 29. The setup to verify the effect of Tx-Rx pair height difference.

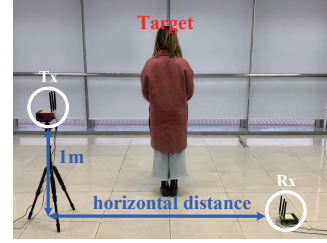
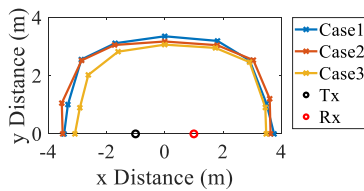
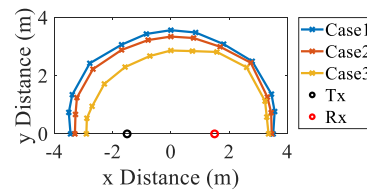


Fig. 30. The experiment setup to verify the effect of Tx-Rx pair height difference on the sensing boundary.



(a) The horizontal distance between Tx-Rx pair is 2 m.



(b) The horizontal distance between Tx-Rx pair is 3 m.

Fig. 31. Experiment results for the effect of Tx-Rx pair height difference on the sensing boundary.

a relatively large value, we need to take the transmitter-receiver height difference into consideration for more accurate sensing coverage estimation.

- **Combining the proposed method with the state-of-the-art signal processing scheme.** Note that the proposed method is a general scheme that can be combined with other advanced signal processing schemes to further improve the sensing coverage. If we apply the advanced signal processing techniques in [39] on top of the proposed transmitter-receiver distance optimization scheme in this work, we can achieve a larger sensing range of 12 m.

6.3 Mitigating Interference for Human Respiration Monitoring

One critical issue of wireless sensing is strong interference because signals reflected from multiple objects get mixed together. Fine-grained respiration monitoring can be easily interfered by surrounding people. We show in this experiment, by properly placing the WiFi transceivers, the interference issue can be significantly mitigated in WiFi sensing. We believe this is one important step towards real-life adoption of wireless sensing.

6.3.1 Methodology. We consider a common scenario in the hospital. As shown in Fig. 32a, two patients can be in the same room. When we monitor the respiration of one patient, the other patient becomes an interferer. Due to the small distance between the target and the interferer, target respiration monitoring can be severely interfered. Fig. 33 shows the respiration pattern with and without interference. It is difficult to extract respiration rate information from the interfered signals. As the interferer can be performing different activities, we consider three interferer activities (i.e., respiration, gesture and walking) as interference. To mitigate the non-target's interference, we consider two different deployment strategies: i) the WiFi transmitter and receiver are both

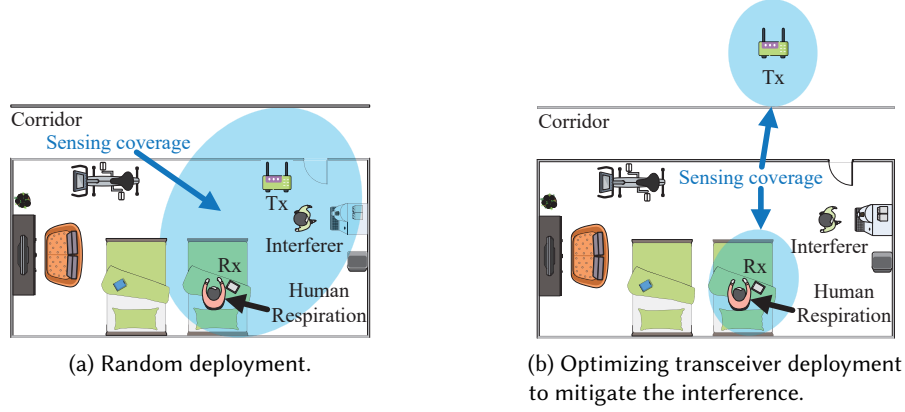


Fig. 32. Increase the LoS path length to mitigate the interference issue for human respiration monitoring.

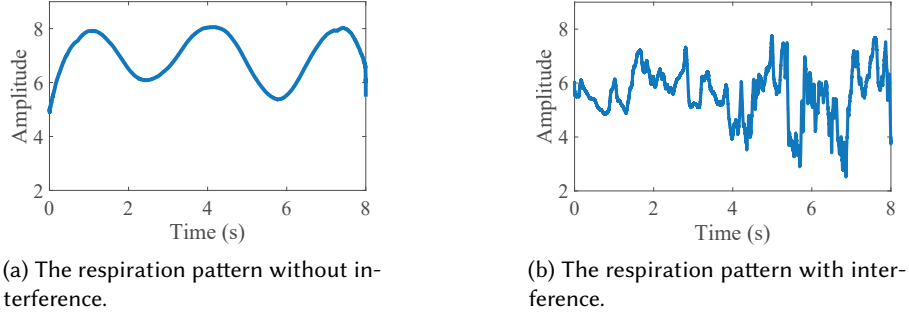


Fig. 33. Respiration sensing can be severely affected by interference.

placed in the ward with a LoS distance of 3 m (Fig. 32a); ii) The transmitter is moved out of the room and the transmitter-receiver distance is 25 m (Fig. 32b).

The ground truth is recorded by Neulog Respiration Monitor Belt logger sensor NUL-236. We employ FFT algorithm to estimate the respiration rate (i.e, breaths per minute, bpm) using the collected CSI samples. The Mean Absolute Error (MAE) is defined as the error between ground truth and estimated rate to quantify the respiration monitoring performance.

6.3.2 Experiment Setting. In this experiment, the transceivers are placed at a height of 0.8 m from the ground as shown in Fig. 34. For deployment strategy 1, both the target and interferer are within the sensing range. For deployment strategy 2, only the target is in the sensing coverage.

- **Overall performance.** We collect a total of 1440 human respiration traces (2 targets × 4 interferers × 3 activities × 2 deployments × 30 times). To show the effect of interference mitigation, we plot the respiration sensing accuracy when the interferer is moved closer to the target when the transmitter-receiver distance is 3 m (deployment strategy 1) and 25 m (deployment strategy 2) respectively. We can see from Fig. 35a that if the interferer is sitting stationary with just respiration, the interferer starts to interfere with the target when the target-distance is 1 m for deployment strategy 1. This value is greatly reduced to 0.5 m

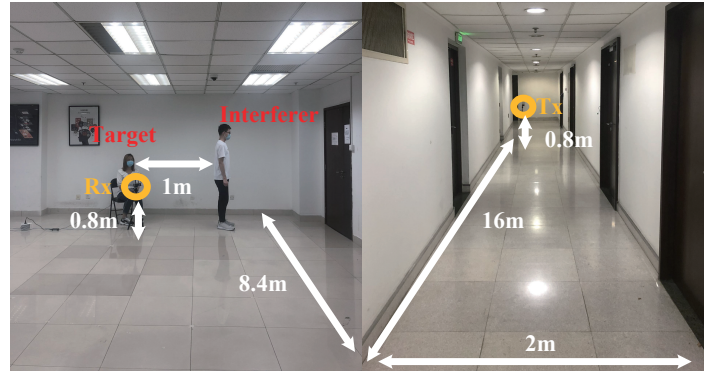


Fig. 34. Respiration sensing in the presence of an interferer. Note that this figure stitches two photos taken at the two sides of the wall into one photo.

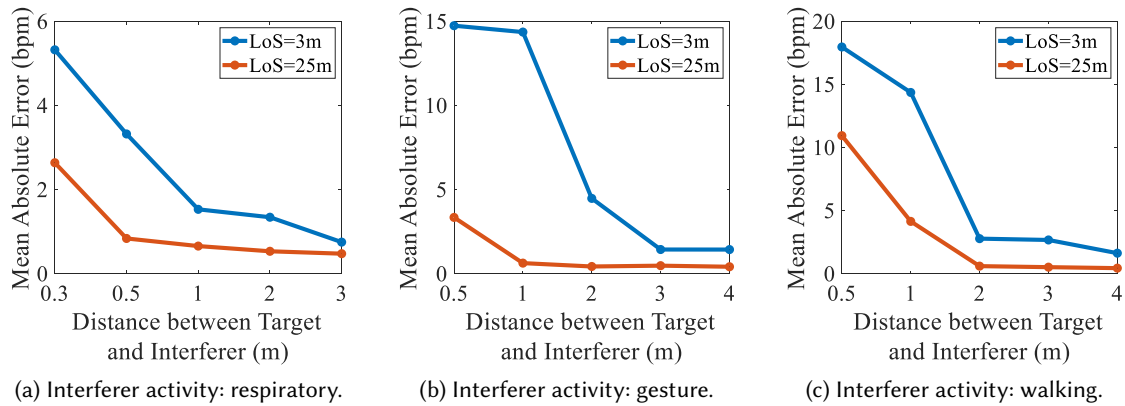


Fig. 35. Employ larger distance to mitigate the effect of interference.

for deployment strategy 2. This means even when the interferer is quite close to the target, it does not interfere with target sensing under the deployment strategy 2. We observe similar result for gesture and walking with the results presented in Fig. 35b and Fig. 35c. We can see that a human interferer performing gestures interferes with target respiration sensing even 3 m away. With the proposed deployment strategy, the target can be as close as 1 m to the interferer without being interfered with. The proposed deployment strategy can therefore significantly mitigate the interference issue. We also notice that walking does bring in more severe interference than respiration and gesture.

- **Impact of LoS path length.** In this experiment, we vary the LoS path length from 10 m to 30 m at a step size of 5 m to see the effect of interference mitigation. In each LoS setting, the interferer sits at a distance of 1 m from the target and breathes naturally. The results are shown in Fig. 36. We observe that the estimation error of respiration rate gradually decreases with the increasing LoS path length. When the LoS path length is more than 10 m, the error is below 1 bpm. The results demonstrate the effectiveness of mitigating interference via increasing the LoS path length.

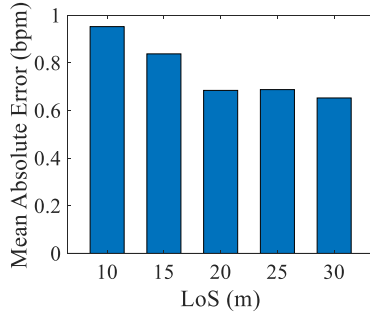


Fig. 36. Impact of LoS path length on the respiration monitoring accuracy.

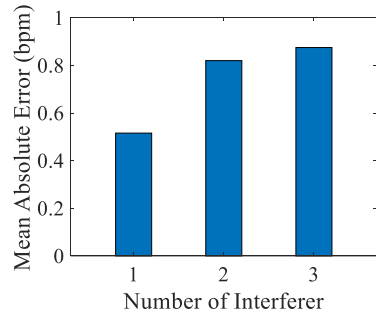


Fig. 37. Impact of number of interferers on the respiration monitoring accuracy.

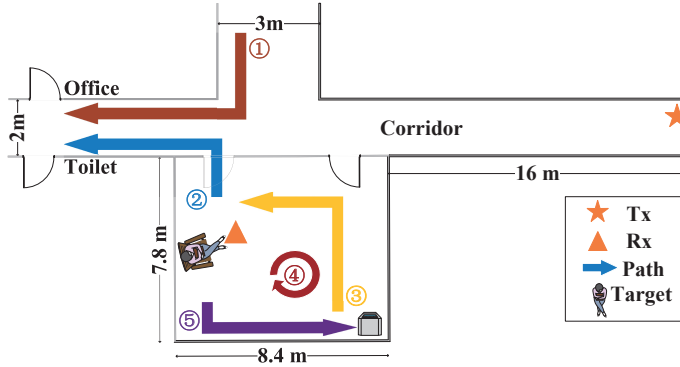


Fig. 38. The experiment setup with the five interferer's moving trajectories marked.

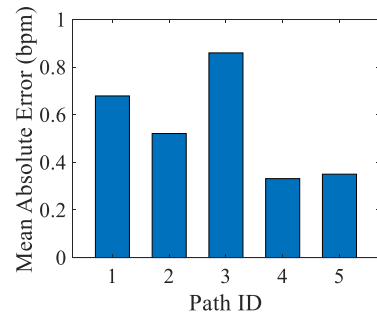


Fig. 39. Impact of interferer's trajectory on the respiration monitoring accuracy.

- **Impact of number of interferers.** We now evaluate the effect of multiple interferers. In this experiment, the participants are asked to walk around the target. Note that walking around generates a larger interference than gesture. The distance between the target and each interferer is around 3 m. Fig. 37 illustrates the errors of respiration monitoring for different numbers of interferers. We observe that although the error increases with more interferers, the error is still below 1 bpm even with three interferers. These results indicate that our approach can effectively mitigate interference.
- **Impact of interferer's trajectory.** To evaluate the effect of the interferer's walking trajectory on respiration sensing, one interferer is asked to walk along five different trajectories including straight lines and a circle (Fig. 38) around the target. Fig. 39 shows that the estimation errors for the five trajectories are 0.67 bpm, 0.52 bpm, 0.85 bpm, 0.33 bpm and 0.35 bpm, respectively. In all five trajectory scenarios, the error is below 1 bpm which satisfies the accuracy requirement for respiration monitoring systems.

7 DISCUSSION AND LIMITATION

Target reflection area. The proposed WiFi sensing coverage model is established without considering the change of the target reflection area. In reality, the target reflection area can vary during the sensing process. Modeling the size of the reflection area of a human target in the process of different activities is challenging.

Fortunately, researchers show that for human walking facing a particular orientation, the target reflection area can be assumed as a constant in a short period [21]. Therefore, we assume the reflection area is a constant in our model and the theoretical results based on this assumption match the experiment results in most scenarios.

Multiple moving subjects. The SSNR metric is simplified to identify the sensing coverage for only one target in the area of interest. In reality, there can be multiple subjects in the area. In this scenario, we can take one subject as target and the other subjects as interferers. One unique opportunity we can leverage to enable multi-subject sensing is that an antenna array is usually equipped at commodity WiFi APs. The multiple antennas can be utilized to separate signals reflected from multiple subjects. In this case, the interference from other subjects can be greatly mitigated, maintaining a high SSNR value and enabling multi-subject sensing.

Implications of the work. The proposed SSNR metric and sensing coverage model can be applied to other wireless systems. However, different wireless technologies do have different SNR thresholds for signal reception. Therefore, the SSNR threshold may also change accordingly for a particular application. In WiFi sensing, an SSNR of 2 dB is required to achieve reliable human tracking. In LoRa sensing, this value needs to be updated due to the chirp design which is capable of obtaining a larger gain at the receiver. Besides fine-grained respiration monitoring, we envision the proposed methods to increase sensing coverage and mitigate interference can be applied to coarse-grained activity sensing and human trajectory tracking as well.

Other measurements. In this paper, we adopt the CSI measurements which can be retrieved from commodity WiFi hardware for sensing. As the proposed methods only employ signal amplitude information to quantify the sensing performance, we believe the results can be generalized to RSSI (received signal strength) and other raw signal measurements. The difference between RSSI and CSI is that CSI contains both phase and amplitude information while RSSI contains only signal strength.

Limitations. While the proposed model works well in 2D, we do observe a relatively large deviation when the transmitter and receiver are located at dramatically different heights (e.g., the WiFi AP is mounted on the ceiling while the WiFi device is placed on the ground). Extending the proposed 2D model to 3D is interesting yet challenging. Also, a few assumptions (e.g., a constant reflection area) are made to simplify our modeling which can cause deviations between the theoretical model and the reality. However, we believe the proposed model does provide general guidance to understand the effect of device placement on sensing.

8 CONCLUSION

In this work, we show that WiFi sensing coverage is closely related to the transmitter-receiver distance. We propose a new metric that can quantify the sensing capability of WiFi systems and theoretically study the effect of LoS path length on sensing coverage. Two case studies are employed to demonstrate how the developed theories could be used to guide the real-world deployment of WiFi sensing systems. The proposed deployment strategy is orthogonal to innovations in other domains (e.g., signal processing and machine learning) and can therefore be combined with other schemes to further improve the sensing performance. We believe this work can help people understand the sensing performance from a different angle and move one step closer to the real life deployment of WiFi sensing systems.

ACKNOWLEDGMENTS

This research is supported by NSFC A3 Project 62061146001, PKU-NTU Collaboration Project, and the Project funded by China Postdoctoral Science Foundation (No. 2021TQ0048).

REFERENCES

- [1] Heba Abdelnasser, Moustafa Youssef, and Khaled A. Harras. 2015. WiGest: A ubiquitous WiFi-based gesture recognition system. In *2015 IEEE Conference on Computer Communications (INFOCOM)*. 1472–1480. <https://doi.org/10.1109/INFOCOM.2015.7218525>

- [2] Roger A. Dana and Dennis L. Knapp. 1983. The Impact of Strong Scintillation on Space Based Radar Design I: Coherent Detection. *IEEE Trans. Aerospace Electron. Systems AES-19*, 4 (1983), 539–549. <https://doi.org/10.1109/TAES.1983.309342>
- [3] Chao Feng, Xinyi Li, Liqiong Chang, Jie Xiong, Xiaojiang Chen, Dingyi Fang, Baoying Liu, Feng Chen, and Tao Zhang. 2018. Material Identification with Commodity Wi-Fi Devices. In *Proceedings of the 16th ACM Conference on Embedded Networked Sensor Systems* (Shenzhen, China) (*SenSys ’18*). Association for Computing Machinery, New York, NY, USA, 382–383. <https://doi.org/10.1145/3274783.3275194>
- [4] Ruiyang Gao, Mi Zhang, Jie Zhang, Yang Li, Enze Yi, Dan Wu, Leye Wang, and Daqing Zhang. 2021. Towards Position-Independent Sensing for Gesture Recognition with Wi-Fi. *Proceedings of the ACM on Interactive, Mobile, Wearable and Ubiquitous Technologies* 5, 2 (2021), 1–28.
- [5] D. Halperin, W. Hu, A. Sheth, and D. Wetherall. 2011. Tool Release: Gathering 802.11N Traces with Channel State Information. *SIGCOMM Comput. Commun. Rev.* 41, 1 (Jan. 2011), 53–53. <https://doi.org/10.1145/1925861.1925870>
- [6] Wenfeng He, Kaishun Wu, Yongpan Zou, and Zhong Ming. 2015. WiFi: WiFi-Based Gesture Recognition System. In *2015 24th International Conference on Computer Communication and Networks (ICCCN)*. 1–7. <https://doi.org/10.1109/ICCCN.2015.7288485>
- [7] R.C. Heimiller, J.E. Belyea, and P.G. Tomlinson. 1983. Distributed Array Radar. *IEEE Trans. Aerospace Electron. Systems AES-19*, 6 (1983), 831–839. <https://doi.org/10.1109/TAES.1983.309395>
- [8] Shengjie Li, Xiang Li, Kai Niu, Hao Wang, Yue Zhang, and Daqing Zhang. 2017. AR-Alarm: An Adaptive and Robust Intrusion Detection System Leveraging CSI from Commodity Wi-Fi. In *Enhanced Quality of Life and Smart Living*, Mounir Mokhtari, Bessam Abdulrazak, and Hamdi Aloulou (Eds.). Springer International Publishing, Cham, 211–223.
- [9] Xiang Li, Shengjie Li, Daqing Zhang, Jie Xiong, Yasha Wang, and Hong Mei. 2016. Dynamic-MUSIC: Accurate Device-Free Indoor Localization (*UbiComp ’16*). Association for Computing Machinery, New York, NY, USA, 196–207. <https://doi.org/10.1145/2971648.2971665>
- [10] Xiang Li, Daqing Zhang, Qin Lv, Jie Xiong, Shengjie Li, Yue Zhang, and Hong Mei. 2017. IndoTrack: Device-Free Indoor Human Tracking with Commodity Wi-Fi. 1, 3, Article 72 (Sept. 2017), 22 pages. <https://doi.org/10.1145/3130940>
- [11] Xuefeng Liu, Jiannong Cao, Shaojie Tang, and Jiaqi Wen. 2014. Wi-Sleep: Contactless Sleep Monitoring via WiFi Signals. In *2014 IEEE Real-Time Systems Symposium*. 346–355. <https://doi.org/10.1109/RTSS.2014.30>
- [12] Kai Niu, Fusang Zhang, Yuhang Jiang, Jie Xiong, Qin Lv, Youwei Zeng, and Daqing Zhang. 2019. WiMorse: A Contactless Morse Code Text Input System Using Ambient WiFi Signals. *IEEE Internet of Things Journal* 6, 6 (Dec 2019), 9993–10008. <https://doi.org/10.1109/JIOT.2019.2934904>
- [13] Kai Niu, Fusang Zhang, Xuanzhi Wang, Qin Lv, Haitong Luo, and Daqing Zhang. 2021. Understanding WiFi Signal Frequency Features for Position-Independent Gesture Sensing. *IEEE Transactions on Mobile Computing* (2021), 1–1. <https://doi.org/10.1109/TMC.2021.3063135>
- [14] Kai Niu, Fusang Zhang, Jie Xiong, Xiang Li, Enze Yi, and Daqing Zhang. 2018. Boosting Fine-Grained Activity Sensing by Embracing Wireless Multipath Effects. In *Proceedings of the 14th International Conference on Emerging Networking EXperiments and Technologies* (Heraklion, Greece) (*CoNEXT ’18*). Association for Computing Machinery, New York, NY, USA, 139–151. <https://doi.org/10.1145/3281425.3281425>
- [15] Neal Patwari and Joey Wilson. 2011. Spatial Models for Human Motion-Induced Signal Strength Variance on Static Links. *IEEE Transactions on Information Forensics and Security* 6, 3 (2011), 791–802. <https://doi.org/10.1109/TIFS.2011.2146774>
- [16] V. Pyati. 1984. The role of circular polarization in bistatic radar for mitigation of interference due to rain. *IEEE Transactions on Antennas and Propagation* 32, 3 (1984), 295–296. <https://doi.org/10.1109/TAP.1984.1143298>
- [17] Kun Qian, Chenshu Wu, Zheng Yang, Yunhao Liu, and Kyle Jamieson. 2017. Widar: Decimeter-Level Passive Tracking via Velocity Monitoring with Commodity Wi-Fi. In *Proceedings of the 18th ACM International Symposium on Mobile Ad Hoc Networking and Computing* (Chennai, India) (*MobiHoc ’17*). Association for Computing Machinery, New York, NY, USA, Article 6, 10 pages. <https://doi.org/10.1145/3084041.3084067>
- [18] Kun Qian, Chenshu Wu, Zheng Yang, Yunhao Liu, and Zimu Zhou. 2014. PADS: Passive detection of moving targets with dynamic speed using PHY layer information. In *2014 20th IEEE International Conference on Parallel and Distributed Systems (ICPADS)*. 1–8. <https://doi.org/10.1109/PADSW.2014.7097784>
- [19] Kun Qian, Chenshu Wu, Zheng Yang, Zimu Zhou, Xu Wang, and Yunhao Liu. 2018. Enabling Phased Array Signal Processing for Mobile WiFi Devices. *IEEE Transactions on Mobile Computing* 17, 8 (Aug 2018), 1820–1833. <https://doi.org/10.1109/TMC.2017.2778155>
- [20] Kun Qian, Chenshu Wu, Yi Zhang, Guidong Zhang, Zheng Yang, and Yunhao Liu. 2018. Widar2.0: Passive Human Tracking with a Single Wi-Fi Link. In *Proceedings of the 16th Annual International Conference on Mobile Systems, Applications, and Services* (Munich, Germany) (*MobiSys ’18*). Association for Computing Machinery, New York, NY, USA, 350–361. <https://doi.org/10.1145/3210240.3210314>
- [21] Merrill Ivan Skolnik. 1980. Introduction to radar systems. New York (1980).
- [22] Merrill I Skolnik. 1990. Radar handbook.
- [23] Bernard D. Steinberg and Eli Yadin. 1982. Distributed Airborne Array Concepts. *IEEE Trans. Aerospace Electron. Systems AES-18*, 2 (1982), 219–227. <https://doi.org/10.1109/TAES.1982.309231>
- [24] David Tse and Pramod Viswanath. 2005. *Fundamentals of Wireless Communication*. Cambridge University Press, USA.

- [25] Fei Wang, Sanping Zhou, Stanislav Panev, Jinsong Han, and Dong Huang. 2019. Person-in-WiFi: Fine-Grained Person Perception Using WiFi. In *2019 IEEE/CVF International Conference on Computer Vision (ICCV)*. 5451–5460. <https://doi.org/10.1109/ICCV.2019.00555>
- [26] Hao Wang, Daqing Zhang, Junyi Ma, Yasha Wang, Yuxiang Wang, Dan Wu, Tao Gu, and Bing Xie. 2016. Human Respiration Detection with Commodity WiFi Devices: Do User Location and Body Orientation Matter?. In *Proceedings of the 2016 ACM International Joint Conference on Pervasive and Ubiquitous Computing* (Heidelberg, Germany) (*UbiComp ’16*). Association for Computing Machinery, New York, NY, USA, 25–36. <https://doi.org/10.1145/2971648.2971744>
- [27] Wei Wang, Alex X Liu, Muhammad Shahzad, Kang Ling, and Sanglu Lu. 2015. Understanding and modeling of wifi signal based human activity recognition. In *Proceedings of the 21st annual international conference on mobile computing and networking*. 65–76.
- [28] Xuyu Wang, Chao Yang, and Shiwen Mao. 2017. PhaseBeat: Exploiting CSI Phase Data for Vital Sign Monitoring with Commodity WiFi Devices. In *2017 IEEE 37th International Conference on Distributed Computing Systems (ICDCS)*. 1230–1239. <https://doi.org/10.1109/ICDCS.2017.206>
- [29] Nicholas J Willis. 2005. *Bistatic radar*. Vol. 2. SciTech Publishing.
- [30] Peder Wolkoff. 2018. Indoor air humidity, air quality, and health – An overview. *International Journal of Hygiene and Environmental Health* 221, 3 (2018), 376–390. <https://doi.org/10.1016/j.ijheh.2018.01.015>
- [31] Chenshu Wu, Zheng Yang, Zimu Zhou, Xuefeng Liu, Yunhao Liu, and Jiannong Cao. 2015. Non-Invasive Detection of Moving and Stationary Human With WiFi. *IEEE Journal on Selected Areas in Communications* 33, 11 (2015), 2329–2342. <https://doi.org/10.1109/JSAC.2015.2430294>
- [32] Dan Wu, Ruiyang Gao, Youwei Zeng, Jinyi Liu, Leye Wang, Tao Gu, and Daqing Zhang. 2020. FingerDraw: Sub-Wavelength Level Finger Motion Tracking with WiFi Signals. *Proc. ACM Interact. Mob. Wearable Ubiquitous Technol.* 4, 1, Article 31 (March 2020), 27 pages. <https://doi.org/10.1145/3380981>
- [33] Dan Wu, Youwei Zeng, Ruiyang Gao, Shengjie Li, Yang Li, Rahul C Shah, Hong Lu, and Daqing Zhang. 2021. WiTraj: Robust Indoor Motion Tracking with WiFi Signals. *IEEE Transactions on Mobile Computing* (2021), 1–1. <https://doi.org/10.1109/TMC.2021.3133114>
- [34] Dan Wu, Daqing Zhang, Chenren Xu, Yasha Wang, and Hao Wang. 2016. WiDir: Walking Direction Estimation Using Wireless Signals. In *Proceedings of the 2016 ACM International Joint Conference on Pervasive and Ubiquitous Computing* (Heidelberg, Germany) (*UbiComp ’16*). Association for Computing Machinery, New York, NY, USA, 351–362. <https://doi.org/10.1145/2971648.2971658>
- [35] Kaishun Wu, Jiang Xiao, Youwen Yi, Min Gao, and Lionel M. Ni. 2012. FILA: Fine-grained indoor localization. In *2012 Proceedings IEEE INFOCOM*. 2210–2218. <https://doi.org/10.1109/INFCOM.2012.6195606>
- [36] Yaxiong Xie, Jie Xiong, Mo Li, and Kyle Jamieson. 2019. MD-Track: Leveraging Multi-Dimensionality for Passive Indoor Wi-Fi Tracking. In *The 25th Annual International Conference on Mobile Computing and Networking* (Los Cabos, Mexico) (*MobiCom ’19*). Association for Computing Machinery, New York, NY, USA, Article 8, 16 pages. <https://doi.org/10.1145/3300061.3300133>
- [37] Tong Xin, Bin Guo, Zhu Wang, Pei Wang, Jacqueline Chi Kei Lam, Victor Li, and Zhiwen Yu. 2018. FreeSense: A Robust Approach for Indoor Human Detection Using Wi-Fi Signals. *Proc. ACM Interact. Mob. Wearable Ubiquitous Technol.* 2, 3, Article 143 (Sept. 2018), 23 pages. <https://doi.org/10.1145/3264953>
- [38] Youwei Zeng, Dan Wu, Ruiyang Gao, Tao Gu, and Daqing Zhang. 2018. FullBreathe: Full Human Respiration Detection Exploiting Complementarity of CSI Phase and Amplitude of WiFi Signals. 2, 3, Article 148 (Sept. 2018), 19 pages. <https://doi.org/10.1145/3264958>
- [39] Youwei Zeng, Dan Wu, Jie Xiong, Enze Yi, Ruiyang Gao, and Daqing Zhang. 2019. FarSense: Pushing the Range Limit of WiFi-Based Respiration Sensing with CSI Ratio of Two Antennas. *Proc. ACM Interact. Mob. Wearable Ubiquitous Technol.* 3, 3, Article 121 (Sept. 2019), 26 pages. <https://doi.org/10.1145/3351279>
- [40] Youwei Zeng, Dan Wu, Jie Xiong, and Daqing Zhang. 2021. Boosting WiFi Sensing Performance via CSI Ratio. *IEEE Pervasive Computing* 20, 1 (Jan 2021), 62–70. <https://doi.org/10.1109/MPRV.2020.3041024>
- [41] Daqing Zhang, Kai Niu, Jie Xiong, Fusang Zhang, and Shengjie Li. 2021. Location Independent Vital Sign Monitoring and Gesture Recognition Using Wi-Fi. *Contactless Human Activity Analysis* 200 (2021), 185.
- [42] Daqing Zhang, Hao Wang, and Dan Wu. 2017. Toward Centimeter-Scale Human Activity Sensing with Wi-Fi Signals. *Computer* 50, 1 (2017), 48–57. <https://doi.org/10.1109/MC.2017.7>
- [43] Diana Zhang, Jingxian Wang, Junsu Jang, Junbo Zhang, and Swaran Kumar. 2019. On the Feasibility of Wi-Fi Based Material Sensing (*MobiCom ’19*). Association for Computing Machinery, New York, NY, USA, Article 41, 16 pages. <https://doi.org/10.1145/3300061.3345442>
- [44] Fusang Zhang, Zhaoxin Chang, Jie Xiong, Rong Zheng, Junqi Ma, Kai Niu, Beihong Jin, and Daqing Zhang. 2021. Unlocking the Beamforming Potential of LoRa for Long-Range Multi-Target Respiration Sensing. *Proc. ACM Interact. Mob. Wearable Ubiquitous Technol.* 5, 2, Article 85 (June 2021), 25 pages. <https://doi.org/10.1145/3463526>
- [45] Fusang Zhang, Kai Niu, Jie Xiong, Beihong Jin, Tao Gu, Yuhang Jiang, and Daqing Zhang. 2019. Towards a Diffraction-Based Sensing Approach on Human Activity Recognition. 3, 1, Article 33 (March 2019), 25 pages. <https://doi.org/10.1145/3314420>
- [46] Fusang Zhang, Daqing Zhang, Jie Xiong, Hao Wang, Kai Niu, Beihong Jin, and Yuxiang Wang. 2018. From Fresnel Diffraction Model to Fine-Grained Human Respiration Sensing with Commodity WiFi Devices. *Proc. ACM Interact. Mob. Wearable Ubiquitous Technol.* 2, 1, Article 53 (March 2018), 23 pages. <https://doi.org/10.1145/3191785>

- [47] Jie Zhang, Zhanyong Tang, Meng Li, Dingyi Fang, Petteri Nurmi, and Zheng Wang. 2018. CrossSense: Towards Cross-Site and Large-Scale WiFi Sensing. In *Proceedings of the 24th Annual International Conference on Mobile Computing and Networking* (New Delhi, India) (*MobiCom '18*). Association for Computing Machinery, New York, NY, USA, 305–320. <https://doi.org/10.1145/3241539.3241570>
- [48] Yue Zheng, Yi Zhang, Kun Qian, Guidong Zhang, Yunhao Liu, Chenshu Wu, and Zheng Yang. 2019. Zero-Effort Cross-Domain Gesture Recognition with Wi-Fi. In *Proceedings of the 17th Annual International Conference on Mobile Systems, Applications, and Services* (Seoul, Republic of Korea) (*MobiSys '19*). Association for Computing Machinery, New York, NY, USA, 313–325. <https://doi.org/10.1145/3307334.3326081>
- [49] Zimu Zhou, Zheng Yang, Chenshu Wu, Longfei Shangguan, and Yunhao Liu. 2013. Towards omnidirectional passive human detection. In *2013 Proceedings IEEE INFOCOM*. 3057–3065. <https://doi.org/10.1109/INFCOM.2013.6567118>
- [50] Hai Zhu, Fu Xiao, Lijuan Sun, Ruchuan Wang, and Panlong Yang. 2017. R-TTWD: Robust Device-Free Through-The-Wall Detection of Moving Human With WiFi. *IEEE Journal on Selected Areas in Communications* 35, 5 (2017), 1090–1103. <https://doi.org/10.1109/JSAC.2017.2679578>
- [51] Vitaliy Zhurbenko (Ed.). 2011. *Electromagnetic Waves*. InTech.